FBAR-CMOS Oscillator Array for Mass-Sensing Applications

Matthew L. Johnston, *Student Member, IEEE*, Ioannis Kymissis, *Member, IEEE*, and Kenneth L. Shepard, *Fellow, IEEE*

***Abstract*—Thin-film bulk acoustic resonators (FBAR) are an effective platform for sensitive biological and chemical detection, where their high operating frequencies make them many times more sensitive than a quartz crystal microbalance. Here, we present a monolithic, solidly mounted FBAR oscillator array on CMOS for mass-sensing applications. Through monolithic integration with CMOS drive circuitry, we aim to overcome the spatial and parasitic load limitations of externally coupled resonators to build dense sensor arrays without specialized fabrication techniques. The sensors in this work are constructed in a 6×4 array atop a 0.18 μm CMOS active substrate, and mass sensitivity comparable to off-chip FBAR sensors is demonstrated.**

***Index Terms*—CMOS, film bulk acoustic resonator (FBAR), mass sensor, sensor array.**

I. Introduction

MULTIPLEXED protein detection is emerging as an important tool for analyzing cellular networks and characterizing complex diseases, where more traditional nucleic acid assays have proven insufficient [1]. Protein microarrays, a primary multiplex detection platform, have already demonstrated efficacy in analyzing and characterizing colon cancer cells [2], breast cancer biomarkers [3], and a myriad of human autoimmune diseases [4]. These technologies are limited, however, by dependence on fluorescently labeled generic binders, where cross-reactivity at the reporter level bounds assay specificity [1]. Additionally, unbound labeled reporters prevent real-time detection and quantification of binding events, as these must be washed away prior to optical interrogation. These limitations can be surmounted with label-free, mass-based sensing techniques, but only if such techniques can overcome their own technological barriers to multiplexed detection.

In gravimetric biomolecular detection, a specific antibody or nucleic acid probe is immobilized on the surface of a mechanical resonator. As target molecules bind to the immobilized probes, the increasing mass causes a decrease in the frequency of the natural mechanical resonance. This resonant frequency can be monitored as a direct indication of bound molecules, eliminating fluorescent labels and allowing real-time interrogation.

The traditional quartz crystal microbalance (QCM) is the most characterized mass-based sensor, where it has long been used to detect antibodies [5] and antigens [6] at sensitivities comparable to traditional labeled immunoassays. In such systems, the natural thickness-mode resonance of a piezoelectric quartz disc is monitored while mass accretes on the functionalized surface. The extent of frequency change per unit mass is proportional to the square of the resonant frequency [6]. This drives a desire for ever-higher resonant frequencies, which are limited by the thickness of self-supporting quartz. Centimeter-scale QCM sensors do not lend themselves to dense integration, limiting them to applications involving a small number of target analytes.

In contrast to traditional megahertz quartz resonators, thin-film bulk acoustic resonators (FBARs) offer significant increases in resonant frequency, typically operating in gigahertz regimes. This translates into a potential sensitivity increase of more than three orders of magnitude over traditional QCM systems, positioning these sensors perfectly for low-concentration biological and chemical sensing applications. FBAR structures have already been shown effective at detecting protein binding [7], antibody-antigen coupling [8], [9], hybridized DNA oligomers [10], [11], and adsorbed gas molecules [12]. Additionally, shear-mode resonators are effective in both air and water, a necessity for real-time biomolecular detection [13]. However, macroscale cabling and microwave instrumentation for gigahertz drive and readout add considerable expense and complexity to the measurement platform and spatially prevent array integration. The alternative, given the micrometer-scale size of FBAR structures, is direct integration of the FBAR with the drive and detection circuitry. Modern CMOS circuits can interface directly with gigahertz transducers to produce small, robust, and inexpensive sensor systems.

In microwave and communication applications, FBAR structures are typically interfaced with active CMOS components through wire-bonding [14], [15], flip-chip [16], and wafer-level [17] connection approaches. While these approaches eliminate complex external instrumentation, spatial limitations still prevent the integration of many sensors into a single system. Building dense mass-sensor arrays requires a shift towards monolithic resonator integration on CMOS, marrying long-held "CMOS-compatible" structures directly with an active CMOS substrate [18].

In this work, we present the first monolithic solidly mounted CMOS-FBAR oscillator array for mass-sensing applications. This fully integrated approach allows for implementation of a

Manuscript received November 06, 2009; revised January 19, 2010; accepted January 19, 2010. Current version published April 02, 2010. This work was supported in part by the National Institute of Environmental Health Sciences under Grant U01ES016074 and in part by the Focus Center Research Program through the C2S2 and MSD Centers. The content is solely the responsibility of the authors and does not necessarily represent the official views of the National Institute of Environmental Health Sciences or the National Institutes of Health. The associate editor coordinating the review of this paper and approving it for publication was Prof. E. H. Yang.

The authors are with the Department of Electrical Engineering, Columbia University, New York, NY 10027 USA (e-mail: mlj@cisl.columbia.edu; johnkym@ee.columbia.edu; shepard@ee.columbia.edu).

Digital Object Identifier 10.1109/JSEN.2010.2042711

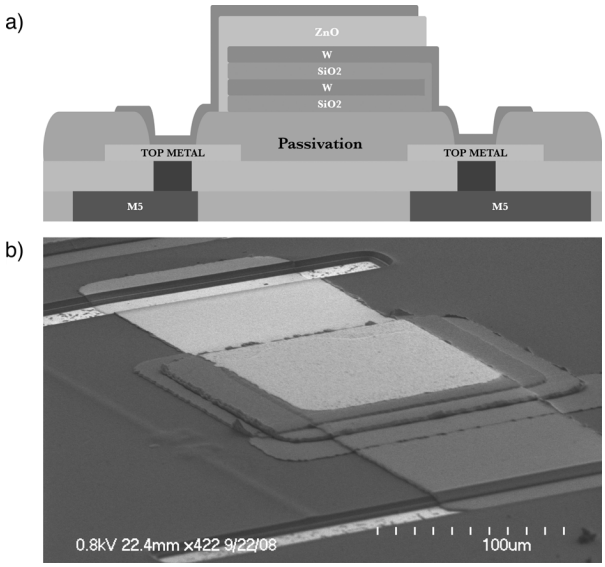

Fig. 1. The solidly mounted FBAR comprises an acoustic mirror (W/SiO2) and a piezoelectric zinc oxide layer on a CMOS integrated circuit substrate, shown both (a) schematically and (b) realized and imaged via SEM micrograph.

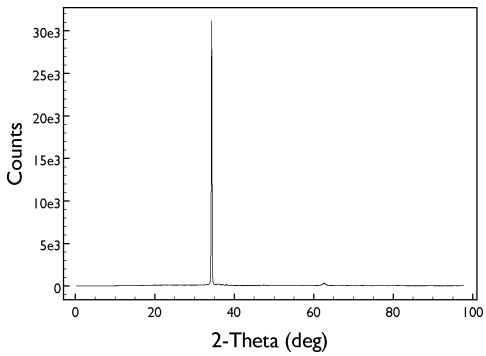

Fig. 2. A peak at 34.4° in the 2θ X-ray diffraction pattern indicates a predominant piezoelectric $\langle 002 \rangle$ c-axis orientation of the sputter-deposited zinc oxide layer.

dense array of sensors directly above its drive circuitry [19]. Such an array of mass sensors, each functionalized for capturing a specific protein, DNA, or gas molecule, will allow simultaneous multiplexed, high-sensitivity measurement of multiple targets on a single sensor chip.

II. FBAR Structure and Materials

A. Piezoelectric Resonator

The FBAR structure comprises a thin layer of piezoelectric material sandwiched between driving electrodes, as shown schematically in Fig. 1(a). The piezoelectric layer is sputter-deposited from a composite zinc oxide target in a 10 milliTorr argon environment at a power of 118 W. Its crystallographic orientation ($\langle 002 \rangle$) is confirmed through a sharp 34.4° peak in the 2θ X-ray diffraction pattern in Fig. 2, which indicates a strong c-axis piezoelectric crystal growth [20]. Top and bottom electrodes are sputter-deposited from a pure tungsten target in a 10 milliTorr argon environment at a power of 208 W. The sputter-deposition process includes single-axis stage rotation and off-axis deposition.

B. Mechanical Isolation

Mechanical resonators must be isolated from a supporting substrate to allow minimally constrained movement. For FBAR devices, this is commonly done using suspended piezoelectric membranes or acoustic reflectors. In the former, the resonator is built atop a sacrificial layer, and this layer is removed via undercut etching, leaving a freestanding membrane resonator [21]. This process can yield very high quality factor (Q) devices, but it requires a chemical undercut process and decreases the structure's mechanical robustness.

Solidly mounted resonators (SMRs), first proposed by Newell in 1967, derive mechanical isolation from a periodic acoustic reflector, analogous to distributed Bragg reflectors in optical systems [22]. Layers of alternating high and low acoustic impedance, each having a thickness equal to one-quarter of the target acoustic wavelength, yield constructive interference at the layer interfaces. In short, most of the mechanical energy ($> 99\%$) is reflected back into the resonator, rather than being dissipated in the supporting substrate. This allows solid, robust, high-Q resonators to be built using a purely additive fabrication processes. In this work, the acoustic reflector is fabricated using alternating layers of sputtered tungsten and silicon dioxide in thicknesses of 650 nm (tungsten) and 750 nm (silicon dioxide). The combined FBAR and acoustic reflector architecture is shown in Fig. 1(a).

III. Active CMOS Substrate

A. FBAR-CMOS Oscillators

Whereas standalone FBAR structures can be characterized with a network analyzer, the resonant frequency of an integrated sensor is more easily measured by using it as the resonant tank of an electrical oscillator. This eliminates the need for complicated frequency sweeps and impedance characterization, and it replicates the method typically used in traditional QCM systems. In this work, active CMOS circuits were used to build integrated FBAR-CMOS oscillators, the output of which can be measured with on-chip or external frequency counters.

The oscillator circuit used follows a standard Pierce oscillator topology, shown schematically in Fig. 3. The inverting amplifier is implemented as three in-line CMOS inverters formed by M1–M6, insuring enough gain to overcome the FBAR material losses and sustain oscillation. M7 serves to bias M1–M6 and its gate voltage can be externally controlled to balance biasing strength with oscillator loading, accommodating variations in FBAR design and construction. C1 and C2 are formed by MIM capacitors set to equal values to promote oscillator startup. The FBAR, whose equivalent Butterworth-Van Dyke circuit model is depicted in the gray box [23], serves as a high-Q resonant tank for the oscillator, and the oscillator output feeds a buffer for entrance into a digital frequency counting circuit.

B. Chip Architecture

The active CMOS substrate supports a 6×4 array of FBAR mass sensors, as well as additional active and passive test sites, as outlined in Fig. 4. The test sites provide for standalone testing of active FBAR-CMOS oscillators and of a passive FBAR resonator, independent of the global power distribution

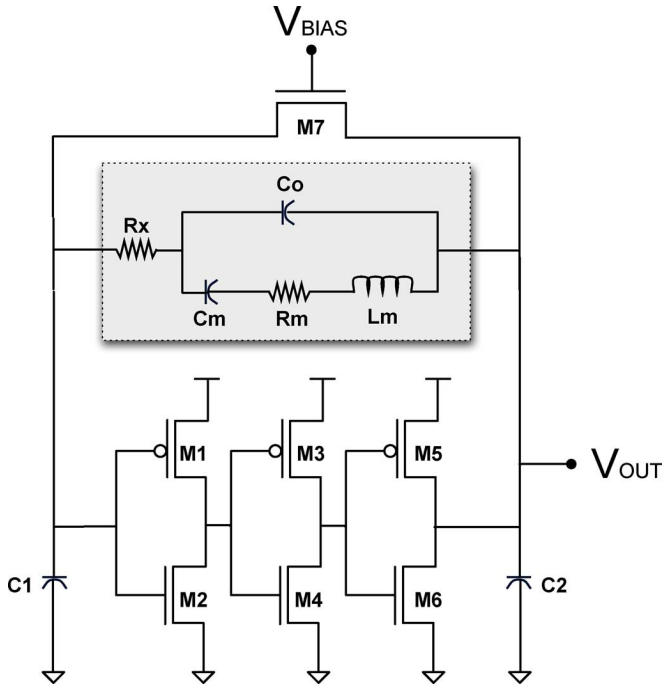

Fig. 3. A single sensor of the global 6×4 FBAR-CMOS array architecture displays the Pierce oscillator topology. The FBAR equivalent circuit model is shown in the grey box, with Cm, Rm, and Lm corresponding to the motional components and Co, Rx corresponding to the intrinsic electrical properties of the zinc oxide structure.

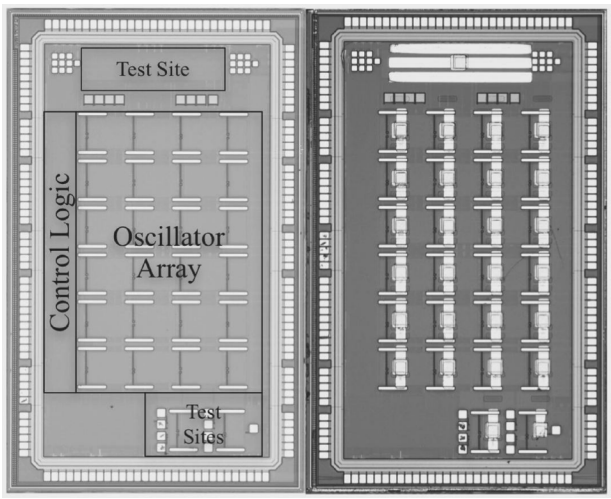

Fig. 4. Left die photo shows CMOS as returned from foundry. Boxes indicate layout of underlying CMOS architecture. Right die photo shows chip after fabrication of FBAR structures, including the passive test structure along the top edge.

and digital control networks. The chips were fabricated in an industrial 0.18 μm RF-CMOS process, and all postprocessing of FBAR devices was performed in-house. The final die size is 3 mm $\times$ 5 mm, and the bare chip can be seen annotated in Fig. 4.

IV. Monolithic FBAR-CMOS Integration

FBAR structures are built atop CMOS dice using the process flow shown in Fig. 5. Bare dice are mounted individually on wafers or glass slides and are patterned lithographically using a

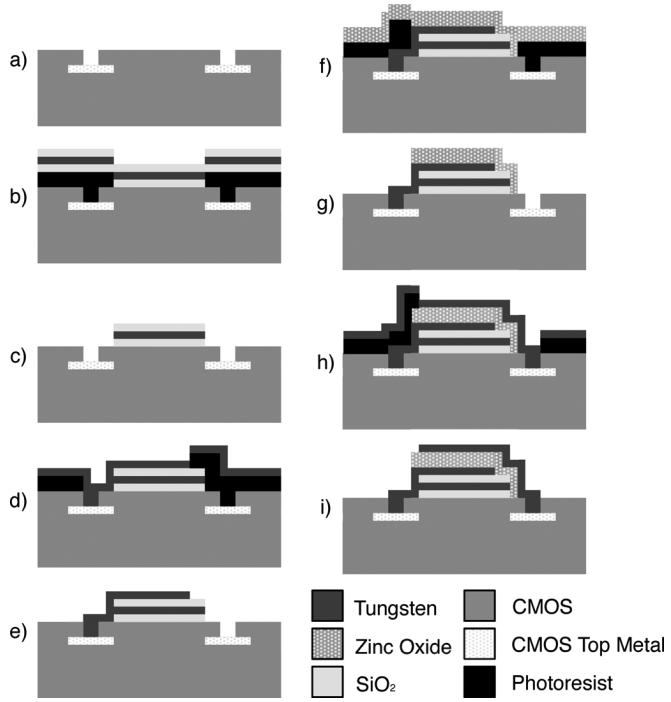

Fig. 5. CMOS post-fabrication of FBAR sensors is shown schematically: (a) a bare CMOS die showing access to top metal through cuts in passivation, (b) and (c) is subject to patterning, deposition, and liftoff of tungsten/silicon-dioxide acoustic mirror, (d) and (e) tungsten FBAR bottom contact, (f) and (g) piezoelectric zinc oxide, and (h) and (i) tungsten FBAR top contact.

thick (6 μm–8 μm) photoresist layer. Exposure times are significantly increased to compensate for the pronounced edge and corner beads that form on small samples. The acoustic reflector layers are sputter deposited, and liftoff proceeds with ultrasonic assist; this also releases a dice from its mounting substrate. This process is repeated to define the bottom electrode (650 nm), piezoelectric layer (1400 nm), and top electrode (200 nm). The zinc oxide overlap depicted in Fig. 5(f)–(i) is used as an insulating layer to prevent electrical shorting through the tungsten reflector layers.

The monolithic sensor array is shown in the right half of Fig. 4, and a micrograph of an on-chip sensor is displayed in Fig. 1(b). Each sensor site occupies 0.13 mm^2, and array density is limited primarily by the area of the FBAR sensors rather than by the area of the underlying circuits. As tested, each resonator comprises a 100 μm$\times$ 100 μm square structure, as defined by the overlap of top and bottom tungsten contacts. Each resonator sits atop an isolated acoustic reflector, rather than sharing a blanket acoustic mirror, to minimize shared acoustic paths and mechanical crosstalk. Optimization of the FBAR size will lead to smaller FBAR footprints and a higher array density in future implementations.

V. Experimental Results

A. FBAR Structures

Individual resonators were fabricated first on glass substrates for independent characterization. These ranged from 80 μm square to 100 μm square and were built with a ground-signal-ground (GSG) probe layout atop a blanket

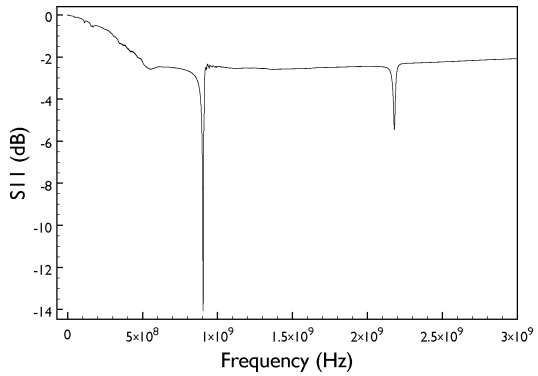

Fig. 6. The return loss of an individual FBAR on glass (without de-embedding) shows a high-Q resonant peak at 905 MHz and a second resonant mode at 2.18 GHz. These correspond to the shear and longitudinal resonant modes, respectively, with quality factors of 113 and 129.

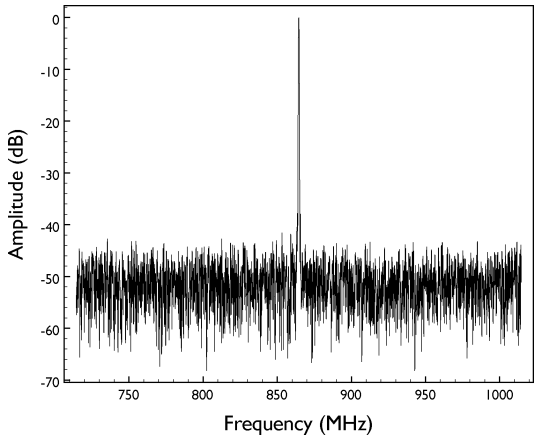

Fig. 7. The output spectrum from monolithic FBAR-CMOS oscillator. This characteristic shows resonance at 864.5 MHz.

four-layer tungsten and silicon dioxide acoustic reflector. Fig. 6 shows the S11 measurement of a single FBAR, demonstrating series resonances at $f_0 = 905\ \mathrm{MHz}$ and $f_0 = 2.18\ \mathrm{GHz}$, which we attribute to shear and longitudinal resonant modes, respectively, of the device. The presence of both modes is consistent with off-axis deposition of the zinc oxide layer [24] and the ratio of the resonance frequencies is in direct proportion to the ratio of the acoustic velocities of these modes. The resonant Q, defined here as $f_0/\Delta f_{\mathrm{FWHM}}$, is 113 for the 905 MHz resonance, and the resonance at 2.18 GHz has a Q of 129. Higher quality factors should be achievable with further tuning of the relative FBAR and acoustic reflector layer thicknesses to achieve better mechanical isolation from the substrate.

B. Monolithic FBAR-CMOS Oscillators

Structures were subsequently built directly atop active CMOS substrates using alternate sputter deposition and photolithographic steps. A completed sensor array is shown in Fig. 4. When supplied with a core voltage of 1.8 V, the completed structures on CMOS oscillate at a frequency corresponding to the lower-frequency shear-mode resonance. This behavior is expected from the lower resonator loss in this mode, and no oscillators we seen to oscillate at the higher frequency mode. The spectrum at the output of one oscillator is shown in Fig. 7, centered at 864.5 MHz. Oscillators across the CMOS array

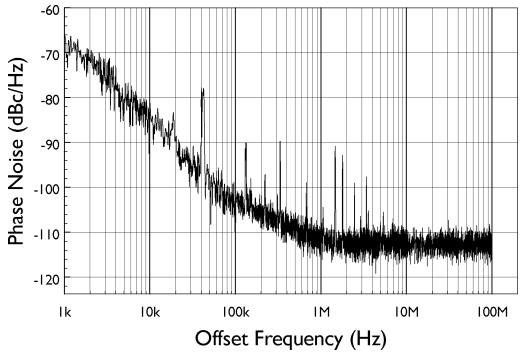

Fig. 8. The phase noise measurement of an array oscillator shows $-83\ \mathrm{dBc/Hz}$ at an offset of 10 kHz and $-104\ \mathrm{dBc/Hz}$ at an offset of 100 kHz.

demonstrate a spread of $\sim 10\ \mathrm{MHz}$ in resonant frequency due to variations in zinc oxide thickness. The phase noise performance of an FBAR-CMOS oscillator is shown in Fig. 8, with a measured noise of $-83\ \mathrm{dBc/Hz}$ at an offset of 10 kHz and $-104\ \mathrm{dBc/Hz}$ at an offset of 100 kHz, both measured from a carrier signal set at the fundamental frequency of oscillation. The relative slope regions of the phase noise plot indicate a loaded Q for the resonator of 218 in accordance with Leeson's empirical phase noise relationship, where a knee at $f_o/2Q$ indicates the transition to a flat, white-noise dominated phase noise response [25].

C. Mass Sensing on FBAR-CMOS Array

Mass detection is demonstrated in Fig. 9 with six different oscillators across the CMOS array. The fundamental oscillation frequency is measured first as a baseline, after which successive layers of patterned $\mathrm{SiO_2}$ are deposited onto the FBAR top surfaces, with frequency measurements taken after each addition. All oscillators that completed the mass series are shown, while those not depicted failed either before or during the testing process (i.e., did not sustain measurable oscillation). The frequency sensitivity of an FBAR to mass additions is given by the Sauerbrey equation

$$\Delta f = \frac{-{f_0}^2 \Delta m}{NA\rho} \tag{1}$$

where f_0 is the operating frequency, $\Delta \mathrm{m}$ is the mass addition, N is the sensitivity constant, A is the active area, and ρ is the density [20]. This equation predicts a linear change in frequency for small additions of uniform mass. From Fig. 9, we calculate an average mass sensitivity of $3.28 \times 10^{11}\ \mathrm{Hz} \bullet \mathrm{cm^2/g}$, which is well above the sensitivity of a typical QCM ($1.7 \times 10^8\ \mathrm{Hz} \bullet \mathrm{cm^2/g}$) [26] and comparable to previous off-chip FBAR sensors [27].

It is clear from Fig. 9 that individual sensors may vary by a few percent in natural resonant frequency (872 to 880 MHz), before mass addition. This can be attributed to both nonuniform zinc oxide thickness and to nonuniform top contact thickness, which leads to different initial mass loading. These variations may be significant in microwave and communication circuits, but for mass-sensing applications only the temporally differential measurement (i.e., before and after mass addition) is used

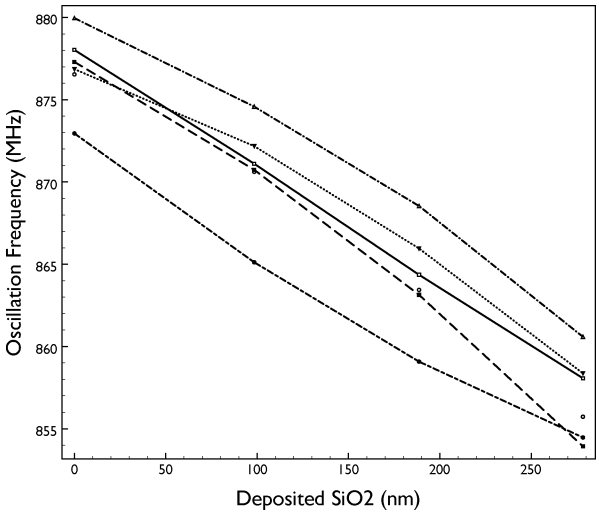

Fig. 9. The mass loading sensitivity is demonstrated on different oscillators in the array; for each oscillator, the resonance decreases linearly with the mass of the deposited silicon dioxide. This data corresponds to a mass sensitivity of 3.3×10^{11} Hz • cm^2/g.

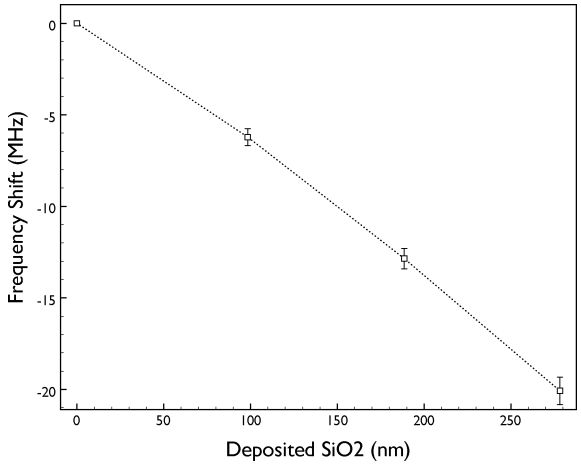

Fig. 10. For mass-based resonant sensors, frequency shift is the target measurement. Subsequently, control and calibration of sensor-to-sensor variability of natural resonance frequency is not critical. Sensors show a sensitivity of 3.3×10^{11} Hz • cm^2/g.

to quantify accreted mass. When used in this manner, as shown in Fig. 10, variation in natural resonance is indiscernible. Error bars in this differential measurement can be attributed in large part to nonuniform deposition of the test masses themselves.

VI. Conclusion

We have demonstrated an array of monolithic FBAR mass-sensors on CMOS for the first time; these exhibit a mass sensitivity of 3.28×10^{11} Hz • cm^2/g, while oscillating around 870 MHz. This implementation overcomes the spatial and parasitic limitations imposed by package-level FBAR integrations and traditional QCMs to enable a dense sensor array. This integration will enable a true multiplexed, label-free biomolecular detection platform unencumbered by intricate and expensive external measurement hardware, and future work will focus on demonstrating such biomolecular viability.

References

[1] P. Angenendt, "Progress in protein and antibody microarray technology," *Drug Discovery Today*, vol. 10, no. 7, pp. 503–511, Apr. 2005.

[2] A. Sreekumar *et al.*, "Profiling of cancer cells using protein microarrays: Discovery of novel radiation-regulated proteins," *Cancer Research*, vol. 61, pp. 7585–7593, Oct. 2001.

[3] Woodbury *et al.*, "Elevated HGF levels in sera from breast cancer patients detected using a protein microarray ELISA," *J. Proteome Research*, vol. 1, no. 3, pp. 233–237, 2002.

[4] I. Balboni *et al.*, "Multiplexed protein array platforms for analysis of autoimmune diseases," *Ann. Rev. Immunol.*, vol. 24, pp. 391–418, Jan. 2006.

[5] A. Shons *et al.*, "An immunospecific microbalance," *J. Biomed. Mater. Res.*, vol. 6, pp. 565–570, 1972.

[6] M. Muratsugu *et al.*, "Quartz crystal microbalance for the detection of microgram quantities of human serum albumin," *Anal. Chem.*, vol. 65, pp. 2933–2937, 1993.

[7] R. Gabl *et al.*, "Novel integrated FBAR sensors: A universal technology platform for bio-and gas-detection," *Proc. IEEE Sensors 2003,* , vol. 2, pp. 1184–1188, Oct. 2003.

[8] G. Wingqvist, J. Bjurstrom, A.-C. Hellgren, and I. Katardjiev, "Immunosensor utilizing a shear mode thin film bulk acoustic sensor," *Sens. Actuators B: Chem.*, vol. 127, no. 1, 2007.

[9] Yan *et al.*, "ZnO-based film bulk acoustic resonator for high sensitivity biosensor applications," *Appl. Phys. Lett.*, vol. 90, p. 143503, 2007.

[10] H. Zhang, M. S. Marma, S. Kamal-Bahl, E. S. Kim, and C. E. McKenna, "Sequence specific label-free DNA sensing using film-bulk-acoustic-resonators," *IEEE Sensors J.*, vol. 7, pp. 1587–1588, 2007.

[11] R. Gabl *et al.*, "First results on label-free detection of DNA and protein molecules using a novel integrated sensor technology based on gravimetric detection principles," *Biosens. Bioelectron.*, vol. 19, pp. 615–620, 2004.

[12] S. Rey-Mermet *et al.*, "Bulk acoustic wave resonator operating at 8 GHz for gravimetric sensing of organic films," *Sens. Actuators B*, vol. 114, pp. 681–686, 2006.

[13] A. Dickherber *et al.*, "Lateral field excitation of thickness shear mode acoustic waves in thin film bulk acoustic resonators as potential biosensor," *Proc. IEEE EMBS*, pp. 4590–4593, 2006.

[14] B. P. Otis *et al.*, "A 300-μW 1.9-GHz CMOS oscillator utilizing micromachined resonators," *IEEE JSSC*, vol. 38, no. 7, pp. 1271–1274, Jul. 2003.

[15] Y. H. Chee *et al.*, "A sub-100 μW 1.9-GHz CMOS oscillator using FBAR resonator," in *Proc. IEEE RFIC Symp.*, 2005, pp. 123–126.

[16] M. Augustyniak *et al.*, "An integrated gravimetric FBAR circuit for operation in liquids using a flip-chip extended 0.13 μm CMOS technology," in *Proc. ISSCC Dig. Tech. Papers*, Feb. 2007, vol. 610, pp. 392–393.

[17] R. C. Ruby *et al.*, "High-Q FBAR filters in a wafer-level chip-scale package," in *Proc. IEEE ISSCC*, 2002, vol. 1, p. 142, 143, 440.

[18] M. Dubois *et al.*, "Integration of high-Q BAW resonators and filters above IC," in *Proc. ISSCC Dig. Tech. Papers*, Feb. 2005, pp. 392–393.

[19] M. L. Johnston *et al.*, "An array of monolithic FBAR-CMOS oscillators for mass-sensing applications," in *Proc. Solid-State Sensors, Actuators and Microsyst. Conf., Transducers*, Jun. 2009, pp. 1626–1629.

[20] J. Rosenbaum, *Bulk Acoustic Wave Theory and Devices*. New York: Artech House, 1945.

[21] Park *et al.*, "Micromachined FBAR RF filters for advanced handset applications," in *Proc. Solid-State Sensors, Actuators and Microsyst. Conf., Transducers*, Jun. 2003, pp. 911–914.

[22] W. E. Newell, "Face-mounted piezoelectric resonators," *Proc. IEEE*, vol. 53, pp. 575–581, 1965.

[23] Aberg *et al.*, "A low noise 0.9 GHz FBAR clock," *Analog Integ. Circ. Sig. Proc.*, vol. 50, no. 2007, pp. 29–37, 2007.

[24] J. Bjurstrom *et al.*, "Synthesis of texured thin piezo- electric AlN films with a nonzero c-axis mean tilt," in *Proc. IEEE Ultrasonics Symp.*, 2005, vol. 1, pp. 321–324.

[25] D. B. Leeson, "A simple model of feedback oscillator noise spectrum," *Proc. IEEE*, vol. 54, pp. 329–330, Feb. 1966.

[26] M. Muratsugu *et al.*, "Quartz crystal microbalance for the detection of microgram quantities of human serum albumin," *Anal. Chem.*, vol. 65, no. 20, pp. 2933–7, Oct. 1993.

[27] Link *et al.*, "Sensing characteristics of high-frequency shear mode resonators in glycerol solutions," *Sens. Actuators: B. Chem.*, pp. 372–378, 2007.

Matthew Johnston (S'06) received the B.S. degree in electrical engineering from the California Institute of Technology, Pasadena, in 2005 and the M.S. degree in electrical engineering from Columbia University, New York, in 2006. He is currently working towards the Ph.D. degree in electrical engineering at Columbia University.

His research interests include piezoelectric mass sensors and the development of CMOS-integrated biosensor platforms. He has held internship positions with the Aerospace Corporation and Cavium Networks, and in 2007 he co-founded Helixis, a Caltech-based startup company. He is currently a member of the Bioelectronics Systems Laboratory at Columbia University.

Ioannis Kymissis (S'97–M'03) received the B.S., M.Eng., and Ph.D. degrees in electrical engineering and computer science from the Massachusetts Institute of Technology (MIT), Cambridge, in 1998, 1999, and 2003, respectively.

He was a Postdoctoral Associate with the Laboratory for Organic Optics and Electronics, MIT, where he was initially engaged in research on the new processing strategies for highly integrated organic systems and, in QDVision, which is a MIT-based startup. He is currently an Assistant Professor with the Department of Electrical Engineering, Columbia University, New York. His research interests include the application of organic FETs to large-area-compatible sensing and actuation systems, and the application of thin-film technology to sensing, display, and large area actuators.

Dr. Kymissis is the Chair of the IEEE New York Section Electron Devices Society/Solid-State Circuits Society Chapter. He has served on the Program Committees of the Materials Research Society, the International Society forOptical Engineers, and several regional conferences. He was the recipient of the IEEE Paul Rappaport Award in 2002 for his contributions to organic FET technology, the Shoulders–Grey–Spindt Medal at the 2002 IVMC for contributions to vacuum microelectronics, and the National Science Foundation CAREER Award in 2006.

Kenneth L. Shepard (M'91–SM'03–F'08) received the B.S.E. degree from Princeton University, Princeton, NJ, in 1987, and the M.S. and Ph.D. degrees in electrical engineering from Stanford University, Stanford, CA, in 1988 and 1992, respectively.

From 1992 to 1997, he was a Research Staff Member and Manager with the VLSI Design Department, IBM T. J. Watson Research Center, Yorktown Heights, NY, where he was responsible for the design methodology for IBM's G4 S/390 microprocessors. Since 1997, he has been with Columbia University, New York, where he is now Professor. He also was Chief Technology Officer of CadMOS Design Technology, San Jose, CA, until its acquisition by CadenceDesign Systems in 2001. His current research interests include carbon electronics, low-power intrachip communication, and CMOS mixed-signal design for biological applications.

Dr. Shepard was Technical Program Chair and General Chair for the 2002 and 2003 International Conference on Computer Design, respectively. He has served on the Program Committees for ISSCC, VLSI Symposium, ICCAD, DAC, ISCAS, ISQED, GLS-VLSI, TAU, and ICCD. He received the Fannie and John Hertz Foundation Doctoral Thesis Prize in 1992, a National Science Foundation CAREER Award in 1998, and the 1999 Distinguished Faculty Teaching Award from the Columbia Engineering School Alumni Association. He has been an Associate Editor of the IEEE TRANSACTIONS ON VERY LARGE-SCALE INTEGRATION (VLSI) SYSTEMS and is currently an Associate Editor for the IEEE JOURNAL OF SOLID-STATE CIRCUITS.